Chapter 5

To study encapsulation of purified phytochemicals and its *in vitro* bioavailability

5.1 Introduction

Extraction and isolation of any natural compound to obtain a specific heath-beneficial effect have always been a great challenge [20]. It is very important to understand the objective of the drug delivery, the physicochemical behavior of the compound, the target location of a drug, and the delivery route to obtain a specific drug's effective functionality [15]. Encapsulation is one of the best techniques to deliver drugs to their target system and protect their maximum functionality [24]. Encapsulation target compound or drug is obtained by enclosing it with several coating materials; natural/synthetic hydrocolloids [5] include gums, natural saccharides, celluloses, proteins, lipids [3], etc. To obtain effective encapsulation, it is also important to understand the drug's nature, encapsulating materials used, and the type of techniques to conduct encapsulation, along with concentrations and parameters of all ingredients. Ion gelation, extrusion, coacervation, and evaporation are some encapsulation techniques that are conducted by using several instruments and apparatus, *viz*., spray dryer, freeze dryer, encapsulator [3], extrusion encapsulation by automatic encapsulator and syringe [27], etc. Encapsulation conditions/parameters majorly affect the quality of microbeads [3]. Encapsulation parameters need to be set to the optimum level to obtain higher efficacy with minimal experimental errors. Metaheuristic techniques such as evolutionary algorithms (e.g. genetic algorithm), swarm intelligence algorithms [16], whale optimization, backtracking algorithms, Jaya algorithm [13], etc. are some increasingly employed frameworks that suggest optimum best solutions for any optimization problems [29]. Ant colony optimization algorithm (ACO) is a heuristic method that functions by the implementation of paradigm via simulation of ants foraging. Bhimkol blossom contains high antioxidant quercetin; a phytochemical belonging to the class of flavonoids, contributing various pharmacological properties [7].

This study contributes to the encapsulation of isolated quercetin rich fraction from bhimkol blossom by using chitosan-alginate polyelectrolyte complex at optimal input parameters set by artificial neural network coupled with ant colony optimization (ANN-ACO) algorithm. To our best knowledge, this is the first research paper on the isolation of quercetin from underutilized bhimkol blossom and the characterization of its encapsulation process. A lack of research has been done on quercetin content in banana

blossoms. The finding of the study investigates the proper encapsulation of high-antioxidant quercetin for efficient target delivery without losing much of its functionality. Microbeads developed in this study will contribute great food industrial and pharmacological applications that can be incorporated in any low-acidic medium to valorize the product's functionality, possibly enhancing its health-beneficial activities.

5.2 Materials and methods

5.2.1 Chemicals and reagents

Chemicals and reagents used in the present study were of high purity analytical grade and the HPLC grade analytical standards and solvents were purchased from Sigma-Aldrich (USA).

5.2.2 Sample preparation

As detailed in the previous Chapter 4, quercetin rich extract (BBQ) was isolated from the bhimkol blossom extract (BBE) by using HPLC.

5.2.3 Encapsulation

As this study was targeted to deliver quercetin to the intestinal route to exhibit some possible pharmacological benefits in the human system, an efficient encapsulation of quercetin was carried out. The ionic gelation method was adopted to encapsulate the quercetin by following the method described by Takka and Gürel [28] with slight modification. A uniform solution was prepared by dissolving quercetin with sodium alginate solution. Chitosan and calcium chloride were dissolved in 3% acetic acid. Then the mixture solution (sodium alginate-quercetin) was added dropwise in a chitosan-calcium chloride solution with a 15 ml syringe.

5.2.4 Optimization of encapsulation

For the optimization of the encapsulation process, Design expert 11 was used to obtain experimental design (Table 5.1) from response surface methodology with Box-Behnken design (RSM-CCD). To prevent the experimental loss in the study, instead of BBQ, quercetin standard (Sigma aldrich, USA) was used for the optimization process. The encapsulation ratio of quercetin: sodium alginate: chitosan: calcium chloride was taken at

1:3:3:1 and the concentration of calcium chloride (5%), encapsulation flow rate (0.2 ml/min), distance from needle to the solution (3 cm) and beaker size (100 ml) were taken as independent fixed variables.

Encapsulation was optimized with the artificial neural network and ant colony optimization (ANN-ACO) in MATLAB-11 [4]. Input layers were concentrations of quercetin (coded as A), sodium alginate (coded as B), chitosan (coded as C), and agitation (coded as D) varying from 0.1 to o.3%, 2 to 4%, 0.5 to 1.5%, and 100-300 rpm, respectively. The encapsulation efficiency (EE%) was taken as the output layer in the experimental design. From the thirteen experimental designs, ACO was introduced for optimization with ANN. The artificial neural network was used to predict the efficiency of the formulation of encapsulation. To train the function, the hyperbolic tangent sigmoid transfer function was used between the input and hidden layers herewith linear transfer function purelin was used between hidden and out layers. ANN network consisted of 4 input layers, 7 hidden layers, and one output layer (Fig. 5.1).

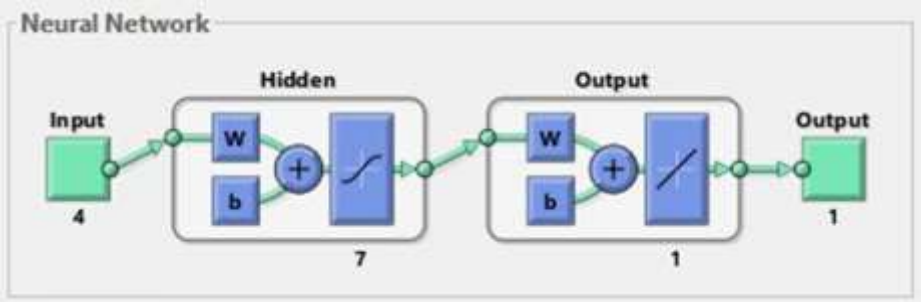

Fig. 5.1 Optimal artificial neural network structure

The algorithm was run by backpropagation with the feed-forward neural network. In training the function the weight and bias iteratively updated Lavenbarg-Marquardt. ANN network was performed for 70% training, 15% for validation, and 15% for testing all datasets. Performance functions were determined by estimating Mean absolute error (MAE), root mean square error (RMSE), mean square error (MSE), mean absolute percentage error (MAPE), and regression of coefficient (R^2) as Equations 1, 2, 3, and 4.

$$MAE = \frac{\sum_{t=1}^{n} |A_t - F_t|}{n} \quad (1)$$

$$MAPE = \frac{\sum_{t=1}^{n} \left| \frac{A_t - F_t}{A_t} \right|}{n} \times 100 \quad (2)$$

$$RSME = \sqrt{\frac{\sum_{t=1}^{n} (A_t - F_t)^2}{n}} \quad 3$$

$$R^2 = 1 - \frac{\sum (A_t - F_t)^2}{\sum (A_t - \bar{F}_t)^2} \quad 4$$

Where, n=17, A_t is experimental value, $F_t$is predicted value

The ant colony optimization (ACO) algorithm is a heuristic algorithm that simulates ants' behavior in foraging and choosing the best optimized root for food in a group with the help of releasing pheromones. A pheromone is a chemical compound that is released by each ant while searching for food through its root, which is automatically read by the others as a communication channel. The shortest distance will contain more concentration of pheromone in the least duration. In this way, the ACO algorithm estimates the shortest optimized path by the ant's information feedback mechanism. When the k^{th} number of ants selects an independent path from the *i* to *j* distance then its probabilistic formula would be $P_{ij}^{k}(t)$ (Equation 5).

$$P_{ij}^{k}(t) = \left\{ \frac{[\tau_{ij}(t)]^{\alpha} [\eta_{ij}]^{\beta}}{\sum k \ \epsilon allowed_k [\tau_{ik}(t)]^{\alpha} [\eta_{ik}]^{\beta}} \right\} \quad 5$$

Where, τ_{ij} is the pheromone density from I to j edge, $\eta_{ij}=(E_{ij}/L_{ij})$ is the heuristic function, E_{ij} is the encapsulation efficiency, L_{ij} is the loading capacity, α and β are the relative importance of pheromone trails or concentration and visibility value (heuristic factors), respectively. Then, $allowed_k$ is the objective function, available state k^{th} ant can select from i^{th} to j^{th} state.

Pheromone updating is performed by reducing the pheromone level to all links to simulate the neural phenomenon of pheromone evaporation and keep all routes equal by the following equation.

$$\tau_{ij}^{new} = \rho \times \tau_{ij}^{old} + \sum_{k}^{K} \Delta\tau_{ij}^{k} \ \ \rho \epsilon (0,1) \quad 6$$

Where, τ_{ij}^{new} (Equation 6) is the pheromone on the link (i,j) after updating, τ_{ij}^{old} is the before updating pheromone on the link (*i*,*j*), ρ is the parameter that controls the speed

of evaporation, *K* is the number of routes in the solution (*K*>0), *k* is the number of routes and $\Delta\tau_{ij}^{k}$ is the increased pheromone found by ants in route *k*. in this experiment, population size (number of ants) was set at 20, and maximum iteration at 40. Initial pheromone τ was set to 1 and ρ at 0.05.

Once optimized conditions of encapsulation of quercetin standard were recorded, finally the BBQ was encapsulated in the encapsulator (Encapsulator Buchi 390, India) at optimized conditions by setting nozzle diameter: 300 µm, flow rate: 10 ml/min, vibration frequency: 1000 Hz, air pressure: 200 mbar, distance between nozzle, and the surface of solution: 15 cm. Microbeads of BBQ obtained at optimized conditions are abbreviated as BBQM and carried out for physicochemical and drug release characteristics.

5.2.5 Physicochemical characterizations of microbeads

5.2.5.1 Encapsulation efficiency and loading capacity

Encapsulation efficiency (EE) of microbeads was estimated by the difference between the total content of quercetin and the amount of residual quercetin content in the supernatant [1]. The quercetin content was estimated as described by Muchahary and Deka [17] with slight modification. The percentage EE was calculated as Equation 7.

$$EE\% = \frac{(Total\ quercetin - Residual\ quercetin)}{Total\ quercetin} \times 100 \qquad 7$$

Loading capacity (LD) was estimated in a percentage ratio of the amount of encapsulated quercetin to the total dry mass of the microbeads (Equation 8).

$$LD\% = \frac{Encapsulated\ quercetin}{Total\ mass\ of\ microcapsule} \times 100 \qquad 8$$

5.2.5.2 Release profiles of quercetin from microbeads

Release characteristics of quercetin from microbeads in three different fluids *viz*., water, simulated gastric fluid (SGF), and simulated intestinal fluid (SIF) were evaluated [6]. A medium of SGF was prepared by dissolving sodium chloride (0.009%) and pepsin (0.003% in 0.01 M hydrochloric acid) finally adjusted to pH 1.5.

The SIF was prepared by dissolving 1.7% of monobasic potassium phosphate, 0.15% of 0.2 N sodium hydroxide, and 10 g of 10% pancreatin, and then the final volume was adjusted up to 1000 ml with distilled water. The medium of SIF is finally adjusted up to pH 6.8 by using sodium hydroxide (0.2 N) and/or hydrochloric acid (0.2 N). Then, microbeads were mixed with SIF in presence of 90 ml of phosphate buffer (pH 6.8).

Microbeads at 50 mg were mixed in 20 ml of water (distilled), SGF, and SIF at 37^{o}C in five different intervals of time from 10 to 60 min with continuous agitation at 50 rpm. Furthermore, each supernatant was collected separately and estimated for quercetin content.

5.2.5.3 Estimation of release efficiency and mean release time of quercetin

Release efficiency (RE) of quercetin from microbeads after 2 h in SGF was estimated from the amount of quercetin released into the fluid at a particular time [1]. The percentage RE of the total amount of quercetin in microbeads was calculated by following Equation 9.

$$RE\% = \frac{Released\ quercetin\ at\ a\ time\ (t)}{Total\ quercetin\ in\ microbeads} \times 100 \qquad 9$$

Mean release time (MRT), the rate of release process was expressed by a regression graph of the amount of quercetin released to the cumulative drug over a given particular time. Physicochemical properties of microbeads *viz*., hygroscopicity (ratio of weight increase of microbeads with initial moisture content to the initial weight increase of microbeads with initial moisture content), bulk density (ratio of the mass of microbeads to the known volume of microbeads), and porosity {1-(bulk density/density of microbeads)} were investigated by following [10].

5.2.5.4 *In vitro* bioavailability study of microbeads

After the quercetin release study in SIF,the fluid was studied for its bioavailavility [23]. Initially, quercetin released SIF fluid obtained at *5.2.5.2* subheading, was quantified for quercetin content. Dialysis membrane (Dialysis tube 150, Av. flat width 37.70 mm, Av. diameter 25.4 mm, pore size- 12 kD, HiMedia) of 15 cm was taken as intestine of the

body and thoroughly washed in phosphate buffer (pH 7.4) to remove extra matters present on it. Dialysis tube was tied in first end and 20 ml of quercetin containing SIF fluid was poured. Without keeping airgap, another end of tube was tied by using clean thread by avoiding any leakage. Then tied dialysis tube was dipped in 50 ml of phosphate buffer (pH 7.4) containing beaker (200 ml) and allowed to release the quercetin content at 37^{o}C, 80 rpm for 2 to 4 h (Fig. 5.2). Intervally, the quercetin content was quantified after 2 and 4 h. The quercetin released after the dialysis was the quercetin amount available for the access by the system of body. The bioavailability was calculated as the ratio of the final release of quercetin content from the dialysis tube in phosphate buffer medium to the initial quercetin content inside the dialysis tube. The experiment was conducted for both quercetin standard (Sigma aldrich) and BBQM, separately.

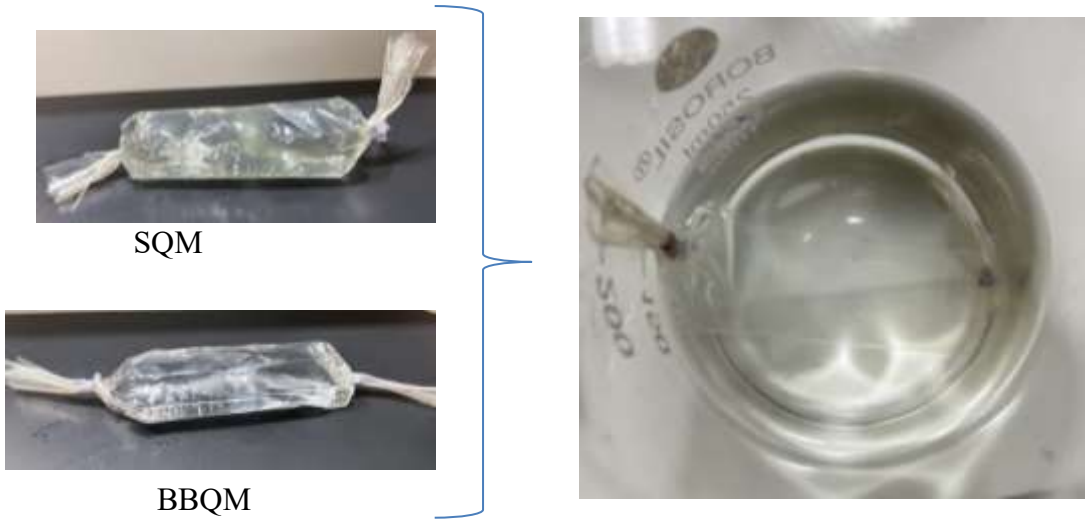

Fig. 5.2 Dialysis of microbeads containing SQM and BBQM in dialysis tubing

5.2.5.5 FTIR and XRD spectra of microbeads

The FTIR spectra of microbeads were obtained similarly as mentioned in the previous Chapter 4 [26]. The powder crystal structure of the BBQM was analyzed by the X-ray diffractometer (Miniflex, Rigaku, Japan). The operation was carried out by following Qi et al. [21] at room temperature (25±5^{o}C) using CuKα radiation (0.15 nm), 185mA, and 50kV over the range 2θ of 5 and 80^{o} with the scanning rate of 1.2^{o}/min.

5.2.6 Morphology of microbeads

5.2.6.1 Scanning electron microscopy

Scanning electron microscopy (SEM) (JEOL, JSM-6390LV, Oxford) images of microbeads were used for examining the microstructure of quercetin loaded in the chitosan alginate complex. Images were recorded at 10 X and 1000 X magnification [22]. The microstructure of microbeads (before dehydration) was also observed in an optical microscope at 10 X.

5.2.6.2 Particle size distribution of microbeads

Particle sizes of microbeads were analyzed by dynamic scattering light, DLS (Particle size analyzer, NanoPlus HD-3, USA) at 25.1^{o}C. The sample of 50 mg BBQM was allowed to disperse in 0.1% basic water (NaOH) and filtered through an 11 µm membrane [22].

5.2.6.3 Molecular interataction of microbead forming complex

Molecular docking of the encapsulating materials were performed in Autodock Vina (PyRx, v0.08) [18]. The molecular structures of encapsulating materials; soldium alginate, chitosan, calcium chloride, and quercetin (derivative; quercetin-3-O-glucoside) were docked. Calcium chloride was taken as the ligand. Binding affifinites of molecular interactions were noted.

5.2.6.4 Storage study of microbeads

Storage study of microbeads (BBQM) was conducted by following Bakowska-Barczak & Kolodziejczyk [2]. Quercetin loss of microbeads over six months at 4^{o}C and 25±10^{o}C in airtight transparent plastic vials were investigated to indirecty study the storage quality of the microbeads. The entire experiment was conducted in triplicates to avoid errors in analyzing the results.

5.3 Results and discussions

5.3.1 Optimization of encapsulation

After the training of 13 experimental runs by ANN-ACO, the best validation performance (2.79) was obtained at epoch 2. The sets of experimental runs were best trained at regression analysis, R at 0.94 training, 0.84 for validation, 0.89 test, and 0.92 for all data sets (Fig. 5.3). The performance functions *viz*., RMSE = 1.48, MSE = 2.2197, R^2 = 0.89, MAE = 0.73, MAPE = 0.01 were obtained. After the 40 iterations of data set, an optimized set of inputs were obtained at A = 0.2%, B = 4%, C = 0.5%, and D = 300 rpm with output 84.54% (EE) (Table 5.1). Performance functions were remarkably efficient, with minimal errors during the training and optimization process. It is well-studied that sodium alginate forms a polyelectrolyte complex with chitosan and calcium chloride when they are dissolved in a suitable medium. The concentration of sodium alginate majorly affected the formation of beads positively. The experiment observed that good firm and rigid beads were formed at and above 2% sodium alginate and calcium chloride 5% at maximum agitation. Chitosan concentration also simultaneously enhanced the coating of the beads with increased EE%. During the encapsulation process, a continuous agitation of solution at optimum rpm also played a major role in building the morphology and EE of the beads. The effects of input parameters over output were observed similarly in line with Li et al. [14]. According to Gu et al. [9] and Samborska et al. [24], chitosan-alginate complex beads formation has better encapsulation characteristics than simple alginate beads.

Table 5.1 Experimental design by response surface methodology (Box-Behnken Design)

Run	A (%)	B (%)	C (%)	D (rpm)	Encapsulation efficiency (EE%)
1	-1	-1	0	0	77.39
2	1	-1	0	0	77.20
3	-1	1	0	0	84.00
4	1	1	0	0	81.52
5	0	0	-1	-1	82.49
6	0	0	1	-1	82.85
7	0	0	-1	1	76.21
8	0	0	1	1	77.26
9	-1	0	0	-1	80.39
10	1	0	0	-1	79.26
11	-1	0	0	1	81.49
12	1	0	0	1	77.11
13	0	-1	-1	0	75.21
14	0	1	-1	0	84.04
15	0	-1	1	0	75.26
16	0	1	1	0	83.58
17	0.1	0	-1	0	80.49
18	1	0	-1	0	79.26
19	-1	0	1	0	82.85
20	0	0	1	0	75.24
21	0	-1	0	-1	82.06
22	0	1	0	-1	84.84
23	0	-1	0	1	78.06
24	0	1	0	1	82.84
25	0	0	0	0	82.06
26	0	0	0	0	82.42
27	0	3	0	0	80.38
28	0	3	0	0	83.80
29	0	3	0	0	83.52

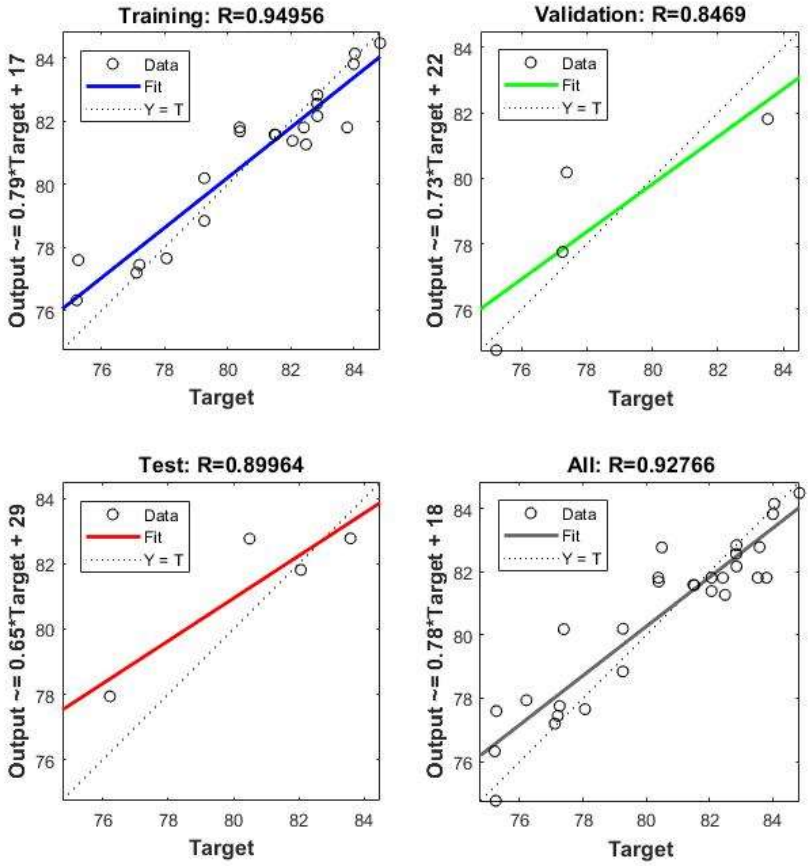

Fig. 5.3 Performance of ANN-ACO for training, validation, test and all data

5.3.2 Characterization of microbeads

Microbeads (BBQM) obtained from the encapsulator at optimized conditions (obtained by ANN-ACO) were found at 200 ± 0.13 µm size, with 85.20 ± 0.23% EE, 11.42 ± 0.17% LD, and 1.35 ± 0.19 mg QE/g microbeads (w/w) quercetin content. Microbeads showed very good efficiency in entrapping the target compound (quercetin). Hygroscopicity, bulk density and porosity were estimated to 9.41± 0.08%, 0.59 ± 0.09 g/cm^3 and 34.15± 0.11%, respectively. Lesser the hygroscopic nature of the microbeads, the better quality of it, which indicates the better storage attributes of the microbeads and protection of the drug inside. Similarly, Lengyel et al. [12] stated that the porosity of the microbeads also indicates the attribute that indicates better vascularization and enhances tissue repair relative to non-pobrous materials.

5.3.2.1 Release profiles of quercetin from microbeads

When any pharmaceutical compound is embedded in any polymer matrix, the behaviour of the polymer matrix is crucial in dissolution and depends on various factors such as release fluid medium, drug properties, and complex formulation [12]. Mean quercetin release at different fluid mediums *viz*., SGF, SIF, and water were observed at different intervals (0 to 60 min) at 37 ± 5 oC. At 60 min, quercetin released from microbeads were 129.24, 68.27, and 1.21 mg/g in SIF, SGF, and water, respectively (Fig. 5.4). This shows that quercetin release depends on the pH level of the medium over the dissolution period. The dissolution profile and permeability of the matrix play a great role in drug release over mediums. The release profile of quercetin from the chitosan-alginate complex was comparatively higher in the SIF (pH 6.8) than in the SGF (1.5) and water. Besides the pH level, the anionic and cationic behaviour of the fluid medium plays an important role in releasing quercetin from the chitosan-alginate matrix. As the target of our study was to sustain maximum gastric medium in the stomach of the human body and functionally active in the target cells located in intestinal lines, developed microbeads showed efficient quercetin release properties. Release efficiency was estimated at 51.696% in SIF and 27.30 % in SGF at 60 min. The MRT obtained from the linear regression curve in SGF was estimated to be 132.00±1.47 min. A controlled release of the drug was observed, similarly, Akolade et al. [1] reported that MRT for drug release from chitosan alginate complex was 118.54±4.63 min in SGF.

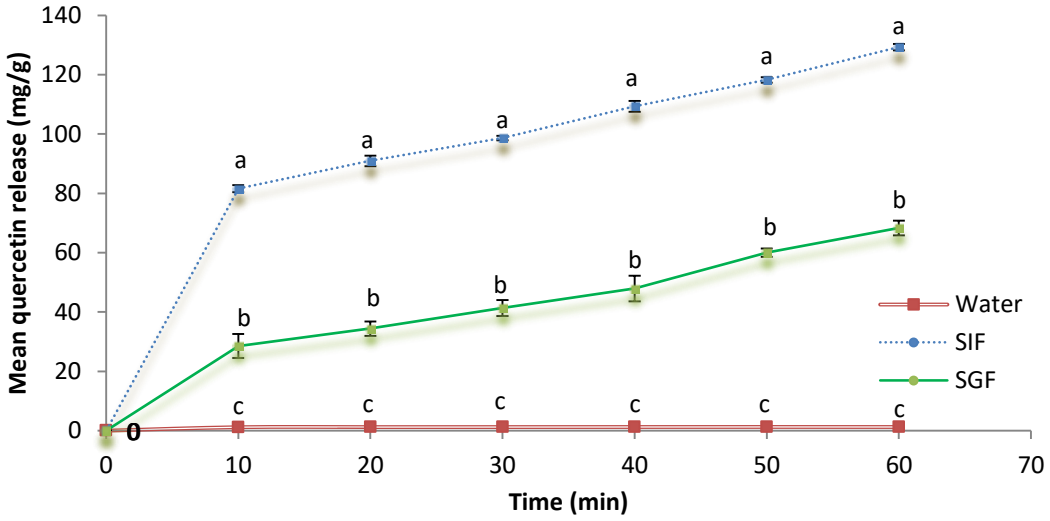

Fig. 5.4 Quercetin release in water, simulated intestinal fluid (SIF) and simulated gastric fluid (SGF)

5.3.2.2 *In vitro* bioavailability study of microbeads

Bioavailabilty of quercetin in microbeads (BBQM) and quercetin standard were illustrated in Table 5.2. The bioavialabilty was seen maximum at 2 h of dialysis in comparison to 4 h of dialysis. Bioavailablity of quercetin in BBQM was observed higher than the quercetin standard. This might be due to the more accessible form of quercetin derivatives present in the BBQM than the quercetin standard. Higher bioavalilabiiy of quercetin indicated the maximum accessible quercetin in the system and greater possibilities of its bioactiviies (*viz*., antioaxidant acitivity, antiimflammatory activity, anticancer, ability to inhibit diabetic enhancing enzymes, reduce cell damage, etc.) [23].

Table 5.2 Bioavailability of quercetin from SIF

Time (h)	Bioavailability (%)	
	Quercetin standard	BBQM
2	1.51±0.01	3.36±0.03
4	0.52±0.00	1.03±0.00

5.3.2.3 FTIR and XRD characterization of microbeads

The FTIR spectra of standard quercetin microbeads (SQM) and bhimkol blossom quercetin microbeads (BBQM) were seen in a similar pattern (Fig. 5.5a). The microbeads quercetin complex (SQM and BBQM) has been observed in broader and curvy peaks than the peaks obtained in FTIR spectra of single quercetin. In BBQM FTIR spectra, a major absorption band has been observed at 3440, 1622, 1422, 1026, and 612 cm^{-1}, similarly in SQM at 3439, 1611, 1422, 1026, and 624 cm^{-1}. The absorbance bands at 3440 and 3439 cm^{-1} were due to OH stretch, 1622 and 1611 cm-1 for H_2O stretch, 1422 cm-1 for symmetric CO_2^- stretch, 1081 to 1026 cm^{-1} for asymmetric C-O-C stretch, and 612 to 624 cm^{-1} are due to the bending vibration of aromatic hydrocarbons [11].

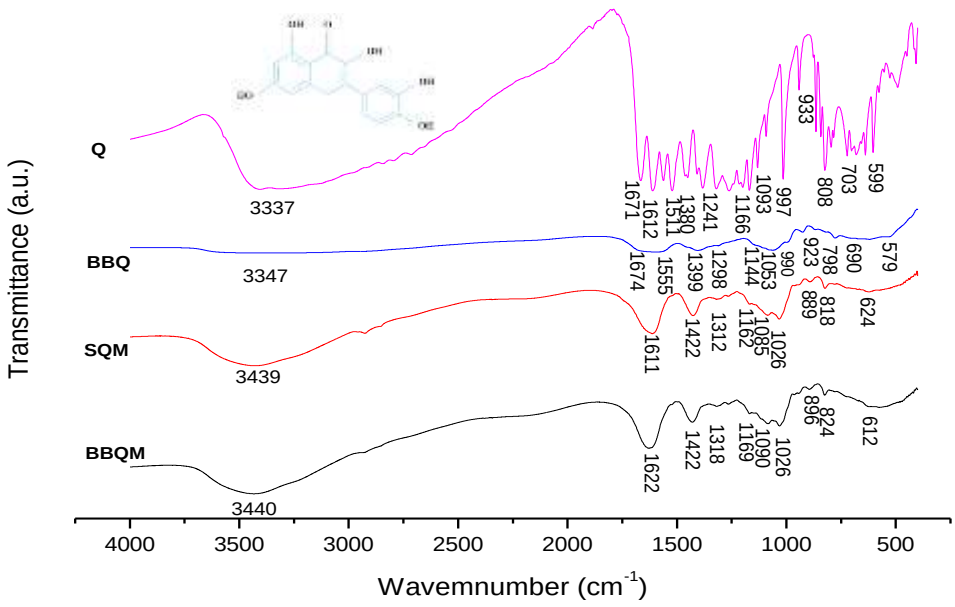

(a)

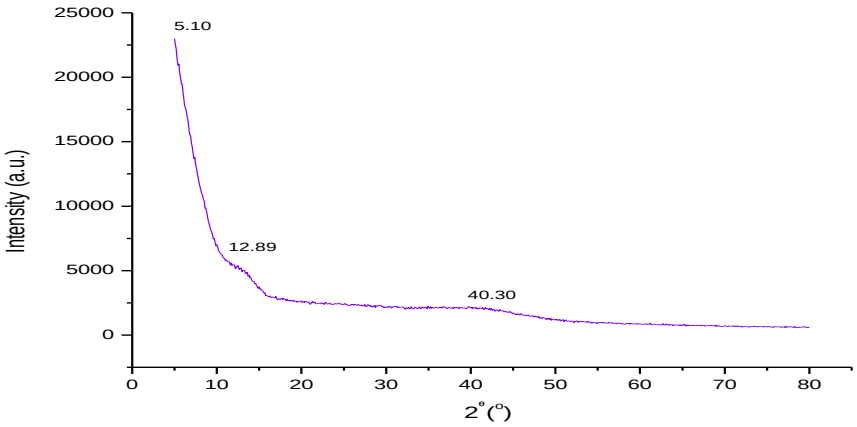

(b)

Fig. 5.5 NMR spectra, FTIR and XRD graphs of quercetin and microbeads; (a) FTIR graph of Q-quercetin, BBQ, SQM-standard quercetin microbeads and BBQM-bhimkol blossom quercetin microbeads and (b) XRD graph of BBQM

The crystallinity of microbeads was revealed by the XRD analysis (Fig. 5.5b). In agreement with Qi et al. [21] and Feng et al. [8], the broad declining curve was observed at 5.10, 12.89, and 40.30^{o} (2θ) demonstrating its non-crystalline behavior. A slight rise was seen from 5.10 to 50^{o} (2θ) and then led to minimal. According to the research

reports, the crystallinity peaks of single compound quercetin rose from around 10.70 to 40.84^{o} (2θ), alginate at around 13 to 40^{o} (2θ), and chitosan at around 20^{o} (2θ), but moreover crystallinity spectra of chitosan alginate complex shows broad curves with non-distinguished peaks. The crystallinity changes with the complex formation and mostly leads to broad curved peaks, however mostly in the case of the carbohydrate-rich complex. This is also due to the gelation process changing the spatial structure of sodium alginate and the intermolecular interactions during the encapsulation process [21, 30].

5.3.3 Morphology of microbeads

From the SEM microstructure of the dehydrated microbeads (quercetin-loaded chitosan-alginate complex), a clear image of the entire surface of the beads can be observed. Shrink-shaped microbeads were observed in the image of dehydrated form (Fig. 5.6a), and a rigid shrined wall of coating material has been observed in Fig. 5.6b.

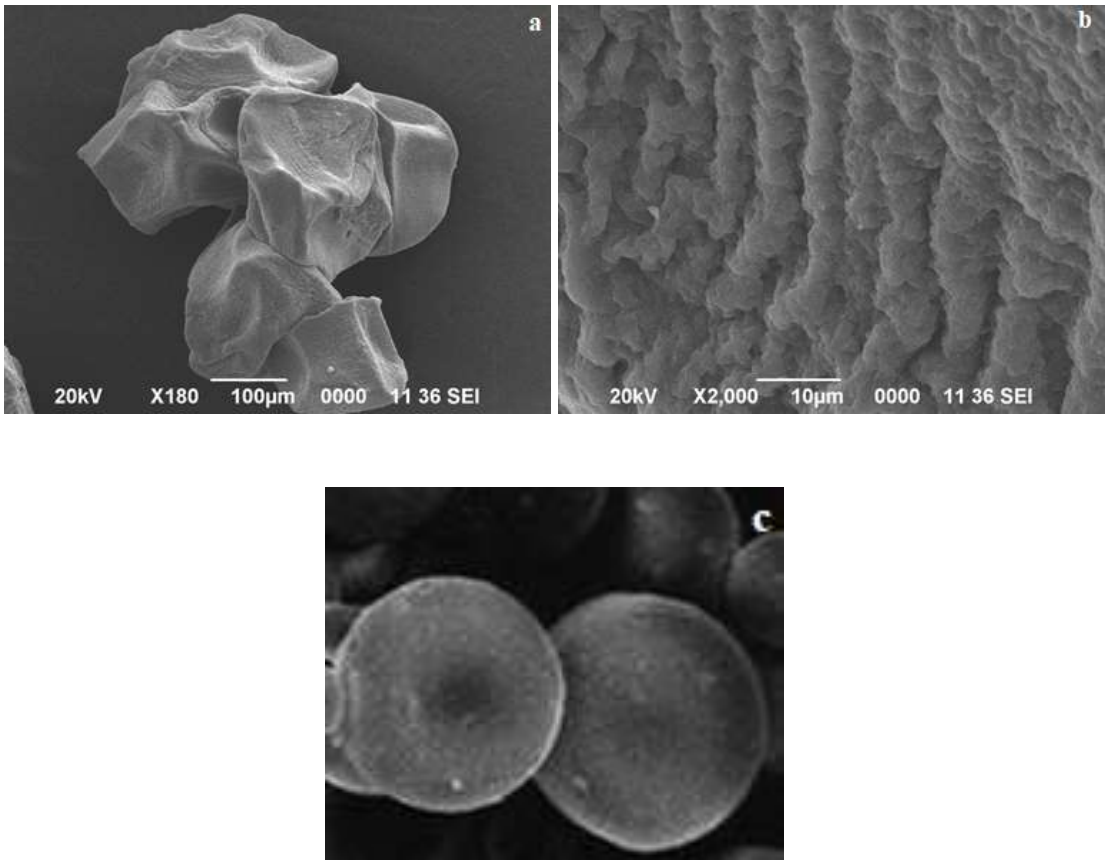

Fig. 5.6 Micrographs of microbeads (bhimkol blossom quercetin microbeads, BBQM): (a) SEM micrograph of dried BBQM (b) SEM micrograph of dried BBQM wall and (c) Optical microscopic image of wet BBQM

A firm spherical surface has been shown in the fresh microbeads observed under an optical microscope (Fig. 5.6c). The complete structure of microbeads depends on the formulation of the coating material used at adopted encapsulation parameters.

5.3.4 Particle size distribution

The size of particles plays an important role in gastrointestinal performance [31]. The DLS detected the average particle size of 2.71µm diameter with a diverse combination of particle ranges.

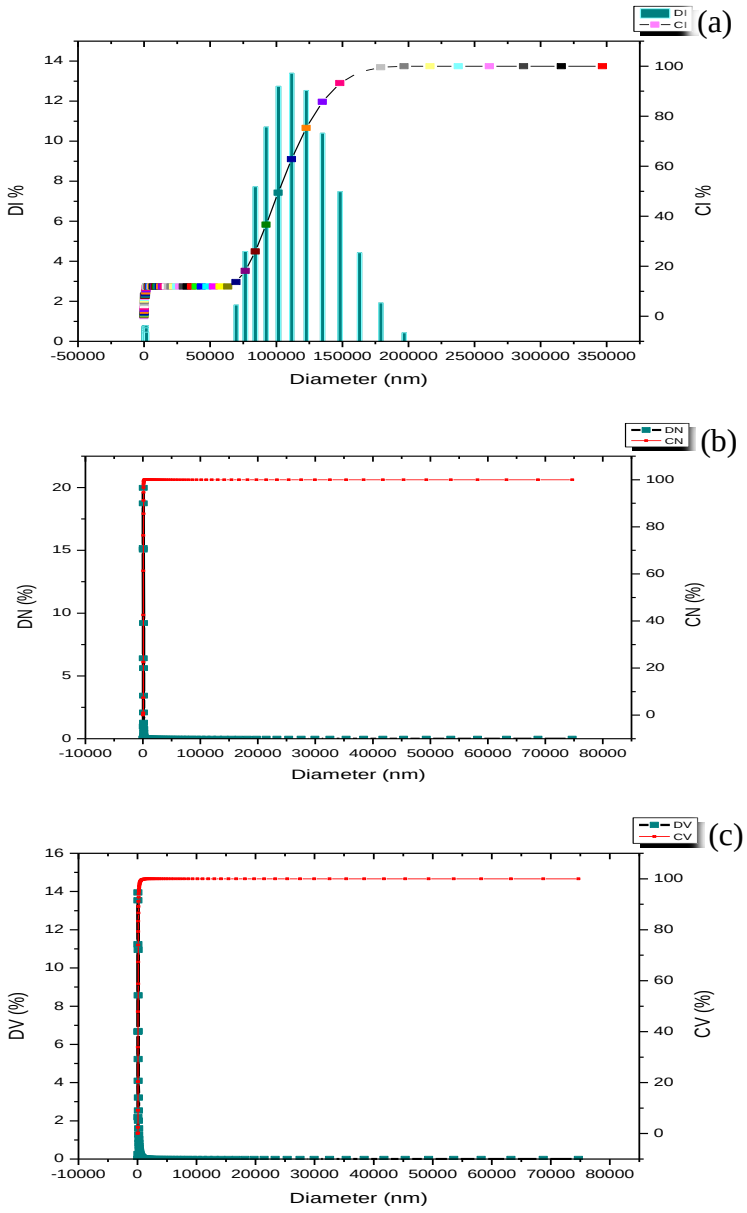

Fig. 5.7 Particle size distribution of microbeads (BBQM- bhimkol blossom quercetin microbeads)

Scattering light intensity according to the sizes (diameters), volumes, and numbers of the particles is shown in Fig. 5.7. Size of the particles up to 200 µm was dispersed at 100% cumulative intensity (CI). The cumulative numbers (CN) and cumulative volume (CV) of particles from 1.5 µm size were observed in 100%. Cumulative percentage is the ratio of cumulative frequency to the total number of observation with multiplied by 100.

The polydispersity index (PDI) of the solution was 0.909. A PDI greater than 0.3 indicates the widely distributed particles in the solution, and a lesser than 0.3 PDI normally tends to have more uniform and stable particles in the solution [2].

5.3.5 Molecular interaction of microbead forming complex

The molecular structure of encapsulating materials, sodium alginate, chitosan, calcium chloride and quercetin were docked as shown in Fig. 5.8. A good binding affinities were observed (Table 5.3).The Ca^{+} ionic crosslinking was observed in the bonds within ligand (calcium chloride) and other molecules. Calcium chloride contains free cations which forms a plyelectrolyte complex when interact with free anions present in alginate and chitosan (N-Succenyl). Ligand bonded with quercetin at glucoside, with alginate by –OH bonding, and with chitosan at first –CH bond. The binding interaction resulted was in line with Mukhopadhyay et al. [18] and Mukhopadhyay et al. [19].

Table 5.3 Binding affinities of encapsulating materials and quercetin

Molecules binding with ligand (Calcium chloride)	Binding Affinity (kJ/mole)
Chitosan	-1.02
Sodium alginate	-1.01
Quercetin	-1.31

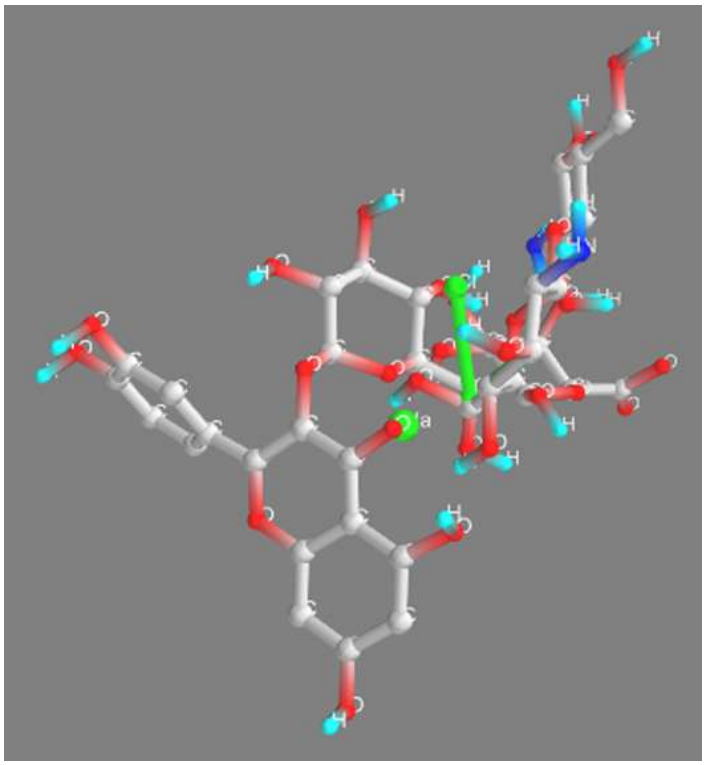

Fig. 5.8 Molecular interaction of encapsulating materials (quercetin derivative + sodium alginate + $CaCl_2$ + chitosan)

5.3.6 Storage study of microbeads

In storage study of microbeads (BBQM), there was no significant quercetin loss in 6 months of study at 4^{o}C (Fig. 5.9). On the other hand, a significant quercetin loss was observed from 2 to 6 months at room temperature (25±10^{o}C). The possible reason of quercetin loss at room temperature despite of microencapsulation might be due to the sunlight penetration causing loss of activities [2]. Therefore, it was concluded that microbeads stored below 25±10^{o}C will execute conserved activity and retain the better shelf life of quercetin in microbeads.

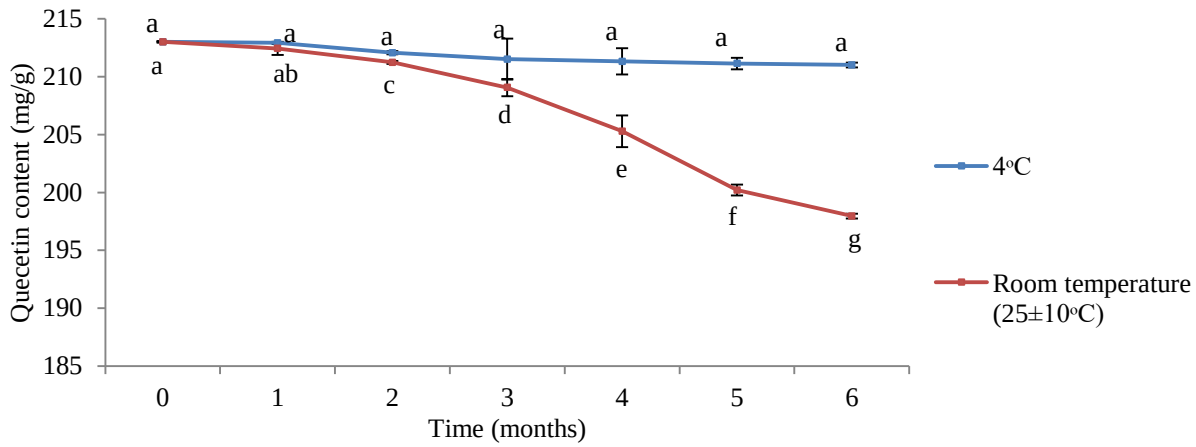

Fig. 5.9 Quercetin loss of BBQM in 6 months. Error bar with different letters are significant different values (p<0.05)

5.4 Conclusions

An effective, optimized encapsulation process is developed from the thirteen experimental (obtained by Box-Behnken design) by artificial neural network coupled with ant colony optimization to obtain an efficient encapsulation of isolated quercetin rich extract with chitosan-alginate polyelectrolyte complex. Increased encapsulation efficiency was obtained by increasing sodium alginate to a significant extent. Similarly, chitosan content and agitation also significantly enhanced the encapsulation efficiency of microbeads up to some extent. Microbeads obtained at optimal encapsulation conditions exhibited high encapsulation efficiency and good drug release characteristics. At the target of our study, microbeads entrapping antioxidant (quercetin) inside will exhibit functional benefits to the cells in intestinal linings after surviving the high acid medium in the stomach. Produced microbeads containing natural quercetin rich fraction will have a vast scope and application in the food industries and pharma sectors. It is further encouraged to conduct and include a detailed study on the health-beneficial properties of microbeads containing natural quercetin rich fraction in the target system.

References

[1] Akolade, J. O., Oloyede, H. O. B., and Onyenekwe, P. C. Encapsulation in chitosan-based polyelectrolyte complexes enhances antidiabetic activity of curcumin. *Journal of Functional Foods*, *35*, 584-594, 2017.

[2] Bakowska-Barczak, A. M. and Kolodziejczyk, P. P. Black currant polyphenols: Their storage stability and microencapsulation. *Industrial Crops and Products*, *34*(2), 1301-1309, 2011.

[3] Ballesteros, L. F., Ramirez, M. J., Orrego, C. E., Teixeira, J. A., and Mussatto, S. I. Encapsulation of antioxidant phenolic compounds extracted from spent coffee grounds by freeze-drying and spray-drying using different coating materials. *Food Chemistry*, *237*, 623-631, 2017.

[4] Beltramo, T., Ranzan, C., Hinrichs, J., and Hitzmann, B. Artificial neural network prediction of the biogas flow rate optimised with an ant colony algorithm. *Biosystems Engineering*, *143*, 68-78, 2016.

[5] Burey, P., Bhandari, B. R., Howes, T., and Gidley, M. J. Hydrocolloid gel particles: formation, characterization, and application. *Critical Reviews in Food Science and Nutrition*, *48*(5), 361-377, 2008.

[6] da Rosa, J. R., Nunes, G. L., Motta, M. H., Fortes, J. P., Weis, G. C. C., Hecktheuer, L. H. R., Muller, E. I., de Menezes, C., R., and da Rosa, C. S. Microencapsulation of anthocyanin compounds extracted from blueberry (*Vaccinium* spp.) by spray drying: Characterization, stability and simulated gastrointestinal conditions. *Food Hydrocolloids*, *89*, 742-748, 2019.

[7] Ezzati, M., Yousefi, B., Velaei, K., and Safa, A. A review on anti-cancer properties of Quercetin in breast cancer. *Life Sciences*, *248*, 117463, 2020.

[8] Feng, R., Wang, L., Zhou, P., Luo, Z., Li, X., and Gao, L. Development of the pH responsive chitosan-alginate based microgel for encapsulation of *Jughans regia* L. polyphenols under simulated gastrointestinal digestion *in vitro*. *Carbohydrate Polymers*, *250*, 116917, 2020.

[9] Gu, L., McClements, D. J., Li, J., Su, Y., Yang, Y., and Li, J. Formulation of alginate/carrageenan microgels to encapsulate, protect and release immunoglobulins: Egg yolk IgY. *Food Hydrocolloids*, *112*, 106349, 2021.

[10] Khawas, P. *Value addition of culinary banana (Musa ABB)*. PhD Thesis, Department of Food Engineering and Technology, Tezpur University, India. 2015.

[11] Lawrie, G., Keen, I., Drew, B., Chandler-Temple, A., Rintoul, L., Fredericks, P., and Grøndahl, L. Interactions between alginate and chitosan biopolymers characterized using FTIR and XPS. *Biomacromolecules*, *8*(8), 2533-2541, 2007.

[12] Lengyel, M., Kállai-Szabó, N., Antal, V., Laki, A. J., and Antal, I. Microparticles, microspheres, and microcapsules for advanced drug delivery. *Scientia Pharmaceutica*, *87*(3), 20, 2019.

[13] Li, S., Gong, W., and Gu, Q. A comprehensive survey on meta-heuristic algorithms for parameter extraction of photovoltaic models. *Renewable and Sustainable Energy Reviews*, *141*, 110828, 2021.

[14] Li, S., Wang, X. T., Zhang, X. B., Yang, R. J., Zhang, H. Z., Zhu, L. Z., and Hou, X. P. Studies on alginate–chitosan microcapsules and renal arterial embolization in rabbits. *Journal of Controlled Release*, *84*(3), 87-98, 2002.

[15] Maleki, A., Kettiger, H., Schoubben, A., Rosenholm, J. M., Ambrogi, V., and Hamidi, M. Mesoporous silica materials: From physico-chemical properties to enhanced dissolution of poorly water-soluble drugs. *Journal of Controlled Release*, *262*, 329-347, 2017.

[16] Mavrovouniotis, M., Li, C., and Yang, S. A survey of swarm intelligence for dynamic optimization: algorithms and applications. *Swarm and Evolutionary Computation*, *33*, 1-17, 2017.

[17] Muchahary, S. and Deka, S. C. Impact of supercritical fluid extraction, ultrasound-assisted extraction, and conventional method on the phytochemicals and antioxidant activity of bhimkol (*Musa balbisiana*) banana blossom. *Journal of Food Processing and Preservation*, *45*(7), e15639, 2021.

[18] Mukhopadhyay, P., Maity, S., Chakraborty, S., Rudra, R., Ghodadara, H., Solanki, M., ... and Kundu, P. P. Oral delivery of quercetin to diabetic animals using novel pH responsive carboxypropionylated chitosan/alginate microparticles. *Royal Society of Chemistry Advances*, *6*(77), 73210-73221, 2016.

[19] Mukhopadhyay, P., Maity, S., Mandal, S., Chakraborti, A. S., Prajapati, A. K., and Kundu, P. P. Preparation, characterization and in vivo evaluation of pH sensitive, safe quercetin-succinylated chitosan-alginate core-shell-corona nanoparticle for diabetes treatment. *Carbohydrate Polymers*, *182*, 42-51, 2018.

[20] Pimentel-Moral, S., de la Luz Cádiz-Gurrea, M., Rodríguez-Pérez, C., and Segura-Carretero, A. Recent advances in extraction technologies of phytochemicals applied for the revaluation of agri-food by-products. *Functional and Preservative Properties of Phytochemicals*, 209-239, 2020.

[21] Qi, Y., Jiang, M., Cui, Y. L., Zhao, L., and Zhou, X. Synthesis of quercetin loaded nanoparticles based on alginate for Pb (II) adsorption in aqueous solution. *Nanoscale Research Letters*, *10*(1), 1-9, 2015.

[22] Qv, X. Y., Zeng, Z. P., and Jiang, J. G. Preparation of lutein microencapsulation by complex coacervation method and its physicochemical properties and stability. *Food Hydrocolloids*, *25*(6), 1596-1603, 2011.

[23] Rodríguez-Félix, F., Del-Toro-Sánchez, C. L., Javier Cinco-Moroyoqui, F., Juárez, J., Ruiz-Cruz, S., López-Ahumada, G. A., Carvajal-Millan, E., Castro-Enríquez, D. D., Barreras-Urbina, C. G., and Tapia-Hernández, J. A. Preparation and characterization of quercetin-loaded zein nanoparticles by electrospraying and study of *in vitro* bioavailability. *Journal of Food Science*, *84*(10), 2883-2897, 2019.

[24] Samborska, K., Boostani, S., Geranpour, M., Hosseini, H., Dima, C., Khoshnoudi-Nia, S., Rostamabadi, H., Falsafi, S. R., Shaddel, R., Akbari-Alavijeh, S., and Jafari, S. M. Green biopolymers from by-products as wall materials for spray drying microencapsulation of phytochemicals. *Trends in Food Science & Technology*, *108*, 297-325, 2021.

[25] Santos, F. H. D., Silveira, B. M. P., Souza, L. L. D., Duarte, A. K. C., Ribeiro, M. C., Pereira, K. C., and Costa, J. M. G. D. Influence of wall materials on the microencapsulation of pequi oil by spray drying. *Brazilian Journal of Food Technology*, *23*, 2020.

[26] Saraswathi, V. S., Saravanan, D., and Santhakumar, K. Isolation of quercetin from the methanolic extract of *Lagerstroemia speciosa* by HPLC technique, its cytotoxicity against MCF-7 cells and photocatalytic activity. *Journal of Photochemistry and Photobiology B: Biology*, *171*, 20-26, 2017.

[27] Shinde, T., Sun-Waterhouse, D., and Brooks, J. Co-extrusion encapsulation of probiotic *Lactobacillus acidophilus* alone or together with apple skin polyphenols: An aqueous and value-added delivery system using alginate. *Food and Bioprocess Technology*, *7*(6), 1581-1596, 2014.

[28] Takka, S. and Gürel, A. Evaluation of chitosan/alginate beads using experimental design: formulation and *in vitro* characterization. *Aaps Pharmscitech*, *11*(1), 460-466, 2010.

[29] Wari, E. and Zhu, W. A survey on metaheuristics for optimization in food manufacturing industry. *Applied Soft Computing*, *46*, 328-343, 2016.

[30] Wu, T. H., Yen, F. L., Lin, L. T., Tsai, T. R., Lin, C. C., and Cham, T. M. Preparation, physicochemical characterization, and antioxidant effects of quercetin nanoparticles. *International Journal of Pharmaceutics*, *346*(1-2), 160-168, 2008.

[31] Zaefarian, F., Abdollahi, M. R., and Ravindran, V. Particle size and feed form in broiler diets: impact on gastrointestinal tract development and gut health. *World's Poultry Science Journal*, *72*(2), 277-290, 2016.